POLITECNICO DI TORINO
Repository ISTITUZIONALE

Multi-Objective Optimization of a Power-to-Power System with Hydrogen Storage in Solid Materials at Room Temperature

Original
Multi-Objective Optimization of a Power-to-Power System with Hydrogen Storage in Solid Materials at Room Temperature / Maurizi, E., Stolte, M., Rozzi, E., Minuto, F.D., Lanzini, A.. - In: HYDROGEN AND FUEL CELLS. - ELETTRONICO. - 1:1(2025).

Availability:
This version is available at: 11583/3003910 since: 2025-10-27T12:46:25Z

Publisher:
Scilight Press

Published
DOI:

Terms of use:

This article is made available under terms and conditions as specified in the corresponding bibliographic description in the repository

Publisher copyright

(Article begins on next page)

27 November 2026

Hydrogen and Fuel Cells
https://www.sciltp.com/journals/hfc

Article

Multi-Objective Optimization of a Power-to-Power System with Hydrogen Storage in Solid Materials at Room Temperature

Elisa Maurizi [1,2], Marcel Stolte [1,2], Elena Rozzi [1,2,*], Francesco D. Minuto [1,2] and Andrea Lanzini [1,2]

[1] Department of Energy, Politecnico di Torino, Corso Duca degli Abruzzi 24, 10129 Torino, Italy
[2] Energy Center Lab, Politecnico di Torino, Via Paolo Borsellino 38/16, 10138 Torino, Italy
* Correspondence: elena.rozzi@polito.it

How To Cite: Maurizi, E.; Stolte, M.; Rozzi, E.; et al. Multi-Objective Optimization of a Power-to-Power System with Hydrogen Storage in Solid Materials at Room Temperature. *Hydrogen and Fuel Cells* **2025**, *1*(1), 3.

Received: 6 August 2025
Revised: 1 September 2025
Accepted: 22 September 2025
Published: 23 September 2025

Abstract: The increasing deployment of variable renewable energy sources calls for scalable and long-duration energy storage solutions. This study investigates the integration of hydrogen storage via physisorption in microporous materials into a Power-to-Power system operating under ambient conditions. A dynamic model is developed to simulate power flows and component interactions, and a multi-objective optimisation is used to minimise both the levelized cost of electricity (LCOE) and grid dependency, with a reference scenario fixed at 20% external electricity withdrawal. Results show that bulk density is the key adsorbent property affecting system performance, while pore volume has a negligible effect. At a material cost of 3.5 € kg^{-1}, high-density metal-organic frameworks (e.g., IRMOF-1 at 500 kg m^{-3}) enable seasonal storage operation at low pressure, achieving LCOE values as low as 0.707 € kW^{-1} h^{-1} and specific hydrogen storage costs of 7.1 € kW^{-1} h^{-1}, below the target of 10 $ kW^{-1} h^{-1}. Conversely, elevated material costs (35 € kg^{-1}) lead to capacity constraints, operation at 350 bar, and increased compressor demand, raising the LCOE to over 0.73 € kW^{-1} h^{-1}. Only selected combinations of material cost and density, such as IRMOF-1 at ≤10 € kg^{-1}, meet cost targets, while MSC-30 remains uncompetitive due to lower hydrogen uptake. These findings underline the importance of reducing MOF synthesis costs and improving packing density. The system exhibits a dual operational role—short-term cycling or seasonal buffering—depending on storage capacity.

Keywords: optimization; hydrogen storage; physisorption; microgrid; techno-economic assessment

1. Introduction

The reduction of greenhouse gas emissions is essential to mitigate climate change and its associated impacts [1]. A substantial transformation of the energy sector is required, given its responsibility for around 85% of global emissions, primarily due to the continued reliance on fossil fuels [2]. This transition requires an expansion of renewable energy sources (RES), which are characterized by enhanced sustainability and reduced carbon footprints in comparison to fossil fuels. Furthermore, it demands advancements in energy efficiency and the fortification of energy security. However, due to the intermittent nature of renewable energy sources, reliable and flexible storage solutions are required to ensure energy stability [3].

In the field of energy storage, lithium-ion batteries have emerged as the dominant technology, owing to their high energy density and efficiency [4]. Their utilization is ubiquitous, encompassing a diverse range of applications,

Copyright: © 2025 by the authors. This is an open access article under the terms and conditions of the Creative Commons Attribution (CC BY) license (https://creativecommons.org/licenses/by/4.0/).
Publisher's Note: Scilight stays neutral with regard to jurisdictional claims in published maps and institutional affiliations.

including portable electronics, electric vehicles, and grid storage. However, while battery energy storage systems (BESS) are highly effective for short- and medium-duration applications, their capital costs become prohibitive when scaled for long-duration storage, rendering them economically unsustainable for seasonal or extended backup scenarios. Supercapacitors have been identified as a potential solution for high-power delivery and rapid cycling applications; however, they remain beyond the scope of this study due to their low energy density and limited relevance for multi-hour storage [5]. This limitation underscores the necessity to investigate alternative storage technologies that are more suitable for long-term energy retention, such as hydrogen-based systems, which involves the utilization of excess electricity to produce hydrogen through the process of electrolysis. Subsequently, hydrogen can be stored and converted back into electricity using fuel cells. This method has been identified as a particularly promising solution for the purpose of long-term and large-scale energy storage, insofar as it facilitates the decoupling of energy production and consumption over extended periods [6]. In contrast to conventional batteries or supercapacitors, hydrogen can be stored for extended periods, rendering it particularly suitable for applications where long-term energy security and system flexibility are required [7].

Hydrogen can be stored in several forms, each of which has specific advantages and limitations. The storage of hydrogen in its gaseous state is typically accomplished by means of compression, a method that has attained widespread prevalence due to the technological maturity and inherent simplicity of the process. It offers relatively high efficiency and fast discharge rates. The utilisation of compressed hydrogen storage has been extensively implemented in both stationary and mobile applications. However, it should be noted that the method is associated with significant trade-offs. It is evident that elevated storage pressures result in a reduction in the necessary tank volume. Nevertheless, this is accompanied by a substantial increase in energy expenditure associated with gas compression and it gives rise to challenges pertaining to the necessity for high-pressure containment systems and associated safety concerns. Operating at lower pressures reduces compression energy demand, but larger storage volumes complicate system integration and logistics. Moreover, even under elevated pressures, the volumetric energy density of compressed hydrogen remains comparatively low in relation to other storage methods, which limits its suitability for applications where space efficiency is critical [8]. Hydrogen can be also stored by liquefaction. Liquefied hydrogen storage, achieved by lowering the temperature of hydrogen to cryogenic levels (i.e., −253 °C), has been demonstrated to significantly increase volumetric energy density when compared with compression; however, the process is energy-intensive and requires sophisticated insulation to minimise boil-off losses [9].

Considering the limitations associated with compression and liquefaction, most notably regarding volumetric energy density and the substantial energy consumption necessitated for gas pressurisation or cryogenic cooling, solid-state hydrogen storage methods are poised to emerge as a promising alternative. These approaches offer the potential for safer, more compact, and energy-efficient storage, particularly in applications where high energy density and ambient operating conditions are desirable. Solid-state hydrogen storage methods can be classified as physical (physisorption) or chemical (chemisorption) storage. Physisorption refers to the reversible, van der Waals binding of H_2 molecules on porous, high-surface-area adsorbents such as activated carbons (AC) or metal–organic frameworks (MOFs). The enthalpy of adsorption for this process is typically within the range of 4 to 10 kJ mol^{-1} H_2 [10], reflecting weak interactions that permit rapid adsorption–desorption kinetics. However, the weak nature of these interactions results in limited storage capacity under ambient conditions [10]. A substantial enhancement in uptake is generally achieved under cryogenic conditions, most commonly at 77 K [11]. Conversely, chemisorption relies on the formation of stronger chemical bonds with metal hydrides or other compounds, thereby enabling higher gravimetric storage densities. However, this approach is hindered by slow kinetics and material degradation over cycles [12].

The optimal hydrogen-storage strategy depends on the application, requiring a balance among energy density, storage duration, efficiency, system complexity, and safety. Consequently, ongoing research endeavours seek to enhance these technologies, with the objective of facilitating the broader implementation of hydrogen in decarbonised energy systems.

Kilic and Altun [13] conducted a comprehensive study on hybrid off-grid renewable energy systems, integrating both battery and compressed hydrogen storage technologies. To this end, they developed dynamic simulation models to evaluate system performance under varying climatic conditions and applied a multi-objective optimization approach—based on the Taguchi method—to minimize levelized cost of energy (LCOE) and CO_2 emissions.

Li et al. [14] developed a comprehensive dynamic model of a hydrogen energy storage system (HESS) for integrated power-to-gas and gas-to-power applications within a microgrid environment. The model, constructed in Simulink, comprises detailed component-level representations of an alkaline electrolyser, a high-pressure hydrogen storage system with a compressor, and a PEM fuel cell. The study analyses hydrogen production,

compression, storage, reconversion processes, and evaluates system performance under varying renewable generation conditions, including interactions with auxiliary battery storage. The findings underscore the prospective function of hydrogen in stabilising renewable-powered microgrids. Moreover, Li et al. [15] developed a detailed simulation model of a large-scale hydrogen storage system, with a particular focus on the effects of capacity attenuation and efficiency degradation. The model considers how internal operating conditions affect system performance. A significant contribution of the study is the incorporation of a degradation model that quantifies capacity loss over time, incorporating both thermal and electrochemical effects. The simulation results illustrate the trade-offs between operating conditions and long-term system reliability. While both contributions provide detailed insights into hydrogen storage systems, they do not address alternative storage mechanisms such as physisorption. In contrast, the study by Minuto et al. [16] explicitly investigates the use of physisorption-based storage at room temperature, highlighting its potential to significantly reduce storage pressure while maintaining competitive round-trip efficiency. The results of the study demonstrate the importance of solid-state storage for ambient conditions and underscore the pivotal role of bulk density in determining performance.

Rozzi et al. [17] developed a detailed dynamic model of a Power-to-Power (P2P) system integrating hydrogen storage via physisorption in microporous materials at room temperature. The present study draws parallels between the performance of the system when utilizing a variety of adsorbents. Furthermore, it provides an evaluation of the impact of thermal management and material properties, including but not limited to pore volume and bulk density, on storage efficiency and round-trip energy performance.

A review of the existing literature revealed no further studies to our knowledge that have incorporated hydrogen physisorption as a storage mechanism within dynamic P2P system models. Existing works predominantly focus on conventional storage technologies, such as compressed hydrogen or metal hydrides, and address system-level behaviour without accounting for the material-specific dynamics of adsorption-based storage. Furthermore, the impact of adsorbent material properties, including pore volume and bulk density, has not been previously incorporated into the system-level design and optimization process.

The novelty of this work lies in the development of a dynamic P2P system model that explicitly incorporates hydrogen storage via ambient temperature physisorption. This is coupled with a multi-objective optimisation framework using a non-dominated sorting genetic algorithm (NSGA-III), which simultaneously considers the trade-off between techno-economic performance and environmental impact. The system sizing is conditioned by the operational behaviour of the system during a full-year simulation. The material-level integration facilitates the refinement of component sizing (e.g., PV array, electrolyser, storage volume and pressure) based on both thermodynamic behaviour and practical energy system requirements. This approach provides a more detailed and realistic evaluation of system performance, enhances cost-effectiveness, and strengthens the applicability of power-to-power hydrogen systems in decarbonised energy networks, particularly for scenarios requiring long-duration storage under ambient conditions.

2. Materials and Methods

This study presents a dynamic model of a P2P energy system which has been designed to support the energy needs of a local energy community. It includes hydrogen storage via physisorption in microporous materials at ambient temperature. The primary objectives are firstly to optimise the system configuration in order to minimise both total costs and dependence on grid electricity, and secondly, to assess the influence of different adsorbent materials on the performance of a physisorption-based hydrogen storage system. The study considers three representative materials: two metal-organic frameworks (IRMOF-1 and NU-110) and one activated carbon (MSC-30). The materials are evaluated and compared against a reference case based on conventional compressed hydrogen storage. This enables an assessment of potential performance and economic advantages. The material cost is treated as a parametric variable. As reported in previous studies, the cost estimates for hydrogen storage materials range from 10 to 70 € kg^{-1} [18,19]. In contrast, the U.S. Department of Energy (DOE) has set a target cost of 10 $ per kilowatt hour for hydrogen storage systems in vehicles [20]. In accordance with the aforementioned points, the present study explores a cost range that is consistent with these benchmarks in order to evaluate the techno-economic feasibility of each material.

The configuration of the system is illustrated schematically in Figure 1. It comprises a photovoltaic (PV) array that supplies electricity to three potential destinations: (i) the community load, (ii) the grid in the event of excess generation and (iii) an electrolyser that converts surplus electricity into hydrogen. The hydrogen that is thus produced is stored in a solid-state physisorption tank at ambient temperature and subsequently reconverted into electricity by a proton exchange membrane fuel cell (PEMFC) to meet the demand when solar production is not sufficient.

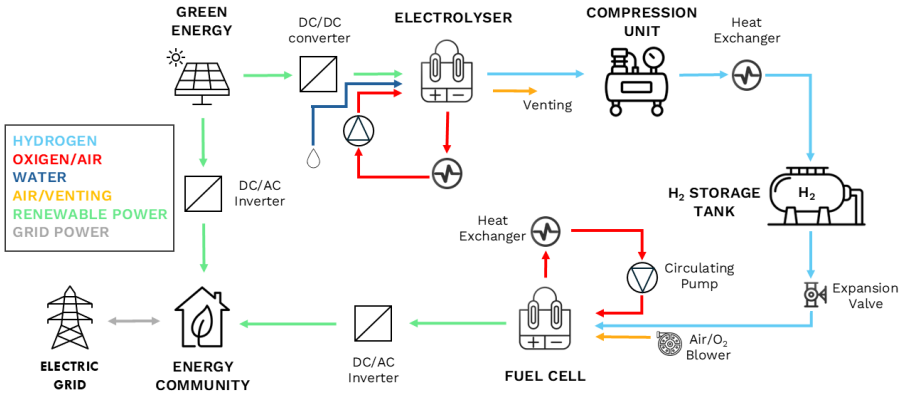


Figure 1. Schematic illustration of the system configuration.

2.1. Simulation Framework

The dynamic behaviour of the P2P system is modelled using mass, energy and power balance equations. These balances are solved over a full calendar year in 30-min time steps to simulate real-time behaviour under varying operating conditions. This approach enables the model to capture both seasonal and daily variations in solar resource availability and load demand. The model includes detailed component submodules for the PV array, the electrolyser, the fuel cell, the physisorption storage system and the electric load. This component modelling approach follows the methodology proposed by Rozzi et al. [17], which includes the modelling of the transient processes involved in hydrogen generation, storage and reconversion, and the thermal management of the electrochemical devices and compression unit.

The dynamic simulation model relies on time-resolved input data representative of real operating conditions including the electric load profile, photovoltaic generation, and time-varying electricity prices. The demand profile is representative of an aggregated electricity consumption of a community based in the north of Italy, derived from empirical measurements of a single apartment's electrical consumption, which are then scaled up accordingly to represent 100 households. The total consumptions add up to an annual electrical load of 192.7 MW h. The photovoltaic generation is computed using site-specific solar irradiance data from PVGIS [21], based on fixed-mounted mono-crystalline modules with default loss assumptions. The price of electricity is determined by the Prezzo Unico Nazionale (PUN), provided by the Italian Energy Market Operator (GME) [22]. A scaling factor of 1.7 is applied to approximate the final retail tariff paid by residential consumers. This correction factor is consistent with typical mark-ups reported in official statistics (e.g., Eurostat) to account for grid charges, non-recuperable taxes, and commercial margins [23]. Figure 2 displays both the full-year profiles and a representative zoom over a five-day period, thereby highlighting typical daily and seasonal fluctuations.

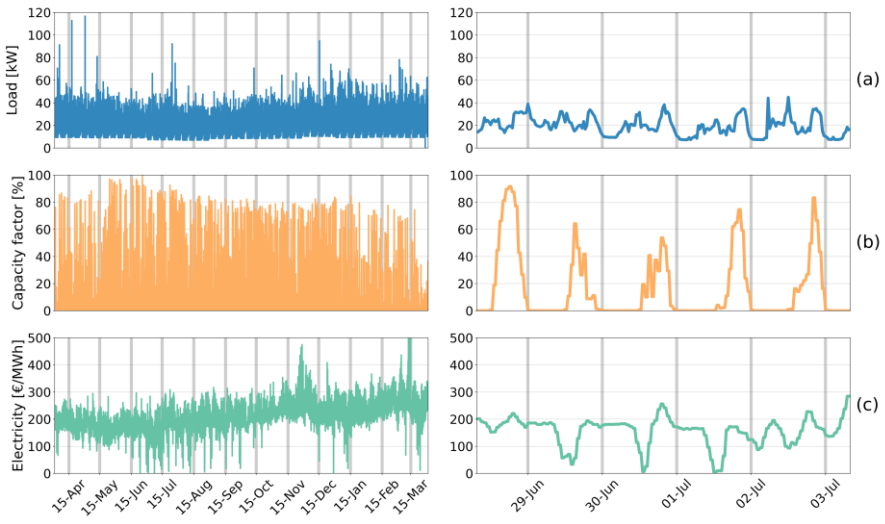


Figure 2. Overview of input datasets utilized in the model: (**a**) Electric load, (**b**) PV generation capacity factor, and (**c**) Time-varying electricity prices. The left panels depict the complete annual profiles for each dataset, while the right panels offer a detailed view of representative fluctuations over a selected 5-day interval.

The operating curves of both the PEM fuel cell and electrolyser were derived by simulating a detailed electrochemical model that captures the realistic performance of each device under varying load conditions. Continuous voltage–current ($V-I$) characteristic curves were reconstructed, enabling accurate estimation of performance across the entire operational range. The relationship between current density and cell voltage is described by polarization curves, which reflect the impact of irreversible losses including activation, ohmic, and concentration overpotentials. The electrochemical efficiencies of the PEM electrolyser (η_{EL}) and the fuel cell (η_{FC}) under nominal operating conditions are assessed, respectively in Equations (1) and (2), using three performance indicators: stack efficiency, Faraday efficiency and system efficiency.

$$\eta_{EL} = \frac{n_{H_2} \cdot LHV}{P_{EL,in} + P_{AUX}} = \frac{\eta_{Faraday} \cdot n_{H_2,id} \cdot LHV}{i \cdot V \cdot N_{cell} \cdot A_{cell} + P_{AUX}} \tag{1}$$

$$\eta_{FC} = \frac{P_{FC,out} - P_{AUX}}{n_{H_2} \cdot LHV} = \frac{i \cdot V \cdot N_{cell} \cdot A_{cell} - P_{AUX}}{n_{H_2,id} \cdot LHV} \eta_{Faraday} \tag{2}$$

where $n_{H_2,id}$ represents the number of moles produced when all current contributes to hydrogen production/utilisation, LHV is the hydrogen lower heating value, i is the current density, V is the cell voltage, N_{cell} is the number of cells, A_{cell} is the cell area.

The electrochemical efficiency of a cell, whether operating in electrolysis or fuel cell mode, can be generally defined as the ratio between the useful energy associated with the desired reaction and the energy exchanged with the system. In the case of the electrolyser, the useful effect corresponds to the chemical energy stored in the form of hydrogen. In contrast, for the fuel cell, it refers to the electrical energy recovered from hydrogen oxidation. The quantification of this ratio is achieved through the use of stack efficiency, a metric that considers only the direct electrochemical conversion process based on the lower heating value of hydrogen.

In order to account for inefficiencies arising from side reactions and parasitic currents, the Faraday efficiency is introduced as a corrective parameter. This parameter quantifies the fraction of electric current that effectively contributes to the intended electrochemical reaction. In this study, the Faraday efficiency ($\eta_{Faraday}$) is modelled in accordance with the empirical approach proposed by Ulleberg [24], which establishes a correlation between efficiency and operating parameters such as current density and temperature, whilst enabling the dynamic adjustment of hydrogen production performance within the simulation model. The efficiency of the system is extended by means of an analysis that incorporates the energy consumed by auxiliary components, including water circulation pumps, fans, cooling, control systems and gas pressurisation units (P_{AUX}). This provides a comprehensive measure of the net energy conversion efficiency of the entire hydrogen production process (Figure 3).

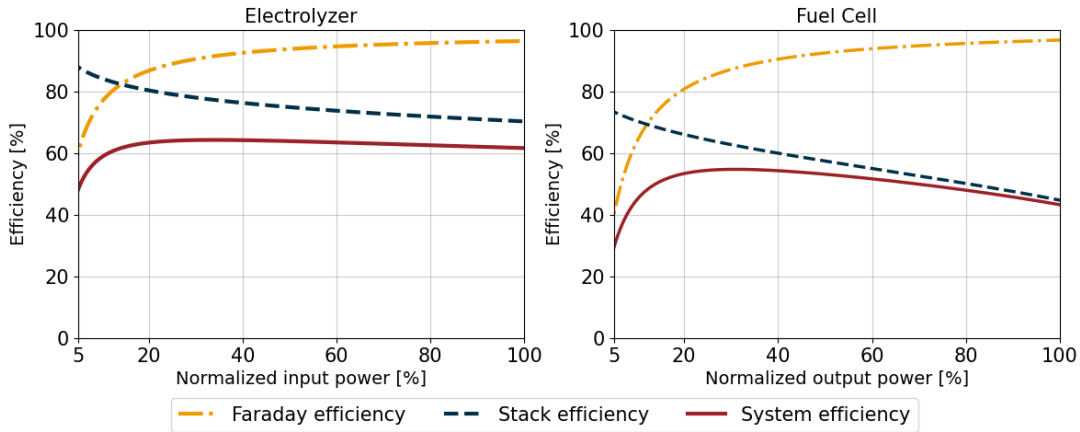


Figure 3. Efficiency curves of the fuel cell (**left**) and of the electrolyser (**right**), evaluated over the operating range from 5% to 100% of nominal capacity.

Concurrently, a scaling relation was formulated to restrict the cell area in accordance with the total rated power of the fuel cell system Figure 4. This relationship serves to prevent the algorithm from assigning unfeasible large active areas at high nominal powers and imposes a realistic, empirically derived mapping between installed capacity and electrode area. The incorporation of this constraint ensures consistency between electrical performance and physical feasibility, whilst also preventing the distortion of optimisation outcomes, especially in

large-scale scenarios. In order to define this relationship, reference data sets by NREL [25] were analyzed. These data sets were then fitted using a power-law function (Equation (3)) [26].

$$A_{cell} = A_{ref} \cdot \frac{P_{ref}}{P_{nom}} \cdot \left(\frac{P_{nom}}{P_{ref}}\right)^{exp} \quad (3)$$

where P_{nom} is the electrolyser nominal power [W]. The fitting parameters include the reference area A_{ref} of 80.85 cm^2, the reference nominal power P_{ref} of 8298 W, and the equation exponent exp of 1.58.

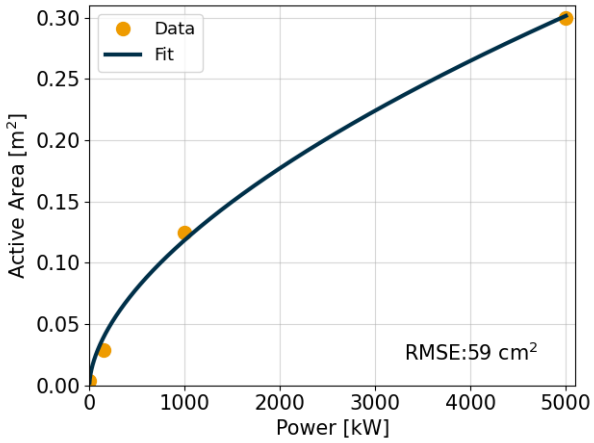


Figure 4. Cell area to total rated power of the fuel cell.

2.2. Physisorption Storage Model

The input data for the hydrogen storage block model comprise the state-of-charge of the storage tank and the hydrogen flow generated by the electrolyser or required by the fuel cell. The outputs of this system are the hydrogen pressure within the tank and the computed storage state-of-charge. To calculate the total amount of hydrogen stored per unit volume of material, the hydrogen adsorption into solid microporous materials is modelled according to the modified Dubinin-Astakhov equations [27]. The excess uptake (n_{exc}) is defined as the difference between the number of moles stored in the adsorbing system at a certain temperature and pressure and the amount of hydrogen that would be present in the absence of the adsorption material at the same thermodynamic conditions. Absolute adsorption (n_{abs}) is defined as the sum of the excess uptake and the number of moles stored in the adsorbate volume. The total amount of gas (n_{tot}) is defined as the sum of the absolute uptake in the adsorbed volume and the total amount of compressed gas within the void volume of the adsorbent [17]. Figure 5 provides a schematic representation of these contributions, illustrating the composition of the total stored hydrogen. This is shown to consist of gas adsorbed in the microporous material and gas present in the void space of the tank. The modelling of absolute isotherms is undertaken in accordance with Equation (4).

$$n_{abs} = n_{max} exp\left[-\left(\frac{RT}{\alpha + \beta T}\right)^2 ln^2\left(\frac{P_0}{P}\right)\right] \quad (4)$$

where n_{max} is the limiting adsorption [mol kg^{-1}] that corresponding to the maximum filling of the whole volume of adsorption space, α is the enthalpic contribution to the hydrogen free-energy of adsorption [J mol^{-1}], β is the entropic contribution to the free energy of adsorption [J mol^{-1} K^{-1})], P is the equilibrium pressure [Pa], and P_0 [Pa] is the pseudo-saturation pressure of the vapor at the storage temperature T [K]. The model parameters (α, β, n_{max}) are determined by means of a non-linear regression analysis of the experimental data for the excess adsorption isotherm. The modelling of excess (5) and total (6) isotherms can be manipulated and written as:

$$n_{exc} = n_{max} exp\left[-\left(\frac{RT}{\alpha + \beta T}\right)^2 ln^2\left(\frac{P_0}{P}\right)\right] \cdot \left(1 - \frac{\rho_{H_2}}{\rho_{liq}}\right) \quad (5)$$

$$n_{tot} = n_{max} exp\left[-\left(\frac{RT}{\alpha + \beta T}\right)^2 ln^2\left(\frac{P_0}{P}\right)\right] + \rho_{H_2} \cdot \left(\frac{1}{\rho_{bulk}} - \frac{1}{\rho_{He}}\right) \quad (6)$$

where ρ_{H_2} is the bulk gas density [mol m^{-3}], ρ_{liq} is the average adsorbed density [kg m^{-3}], ρ_{bulk} [kg m^{-3}] is the bulk density and ρ_{He} [kg m^{-3}] is the open-pore density determined by helium pycnometry.

The bulk density, also referred to as packing or apparent density, is defined as the measure of the density of a material when it is in a compacted state. It is calculated as a function of the skeletal and the pore volume. The volumetric hydrogen storage capacity of an adsorbent material is calculated by multiplying the total adsorption by its bulk density. These physical parameters directly shape the adsorption isotherm, thereby determining the overall hydrogen storage potential within a tank volume.

In this study, three distinct adsorbent materials are evaluated: two metal-organic frameworks (MOFs) (IRMOF-1 and NU-110) and one activated carbon (MSC-30). The selection of these materials was made on the basis of their prominence in the relevant literature and the availability of detailed characterisation data [28,29]. The values of bulk density that were utilized were derived from a previously published dynamic system model, in which the same materials were evaluated under realistic conditions [17]. As illustrated in Figure 6a, the distinct combinations of pore volume and bulk density inherent to each material result in different volumetric uptake profiles. It is noteworthy that IRMOF-1, which attains both high pore volume and moderate bulk density, has been shown to achieve the highest volumetric storage capacity of the three materials under investigation, particularly at elevated pressures. Given the significant variability reported for the properties of these materials, a sensitivity analysis has been performed to study how these parameters might influence the optimization results. Figure 6b extends the analysis by exploring a broader range of pore volume and bulk density combinations for IRMOF-1. The parameter ranges used in this analysis are summarized in Table 1. For both bulk density and pore volume, minimum and maximum values were identified across different studies [28–32], while the third reference point was calculated as the arithmetic mean between these two extremes. An increase in bulk density enhances the mass of material per unit volume, while a larger pore volume raises adsorption capacity. Collectively, these variations result in significant increases in volumetric hydrogen uptake.

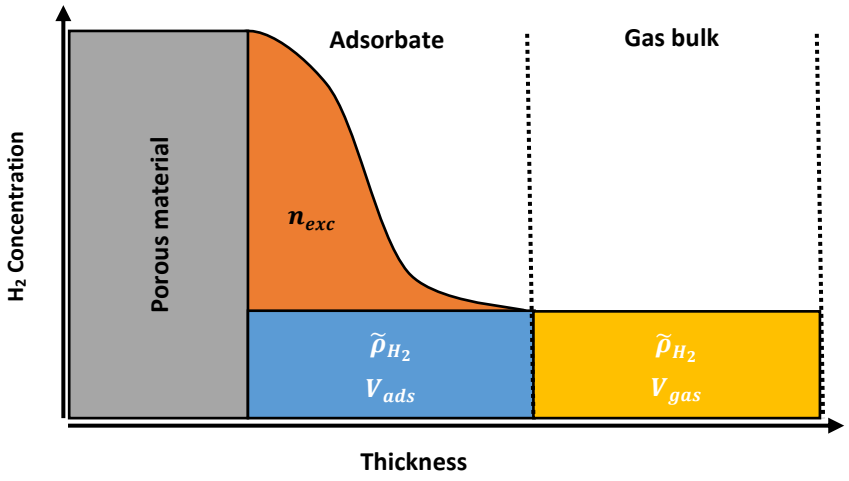


Figure 5. Contributions to the total stored hydrogen.

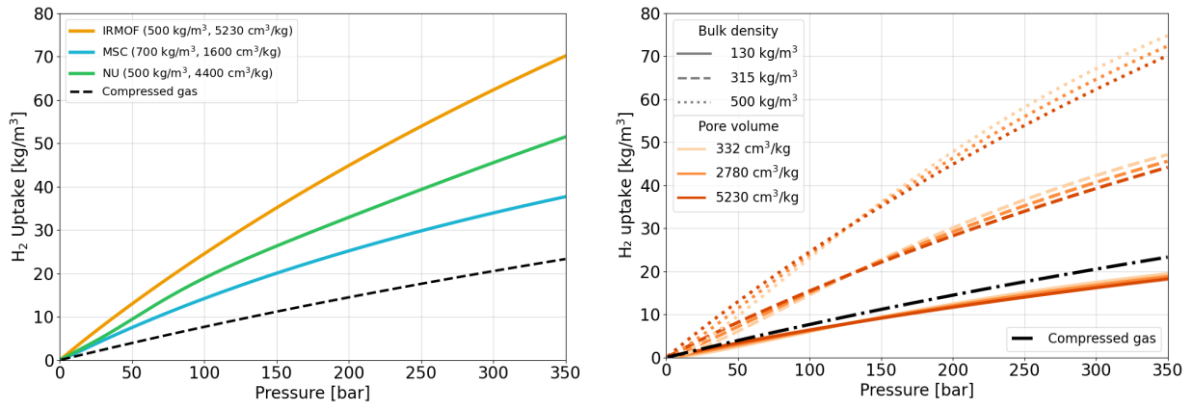
Table 1. Minimum and maximum values for pore volume and bulk density assumed in the analysis.

Pore Volume		
Min	332 $cm^3\ kg^{-1}$	[30]
Max	5230 $cm^3\ kg^{-1}$	[31]
Bulk Density		
Min	130 $kg\ m^{-3}$	[32]
Max	500 $kg\ m^{-3}$	[32]

The physisorption hydrogen storage is compared to a compressed-hydrogen storage. The pressure in a pressurised storage tank is evaluated as a function of the stored hydrogen density ($\rho_{H2,storage}$) and temperature. The molar density of the hydrogen stored is calculated for each time step as (7).

$$\rho_{H2,storage} = \frac{N_{H2,storage}}{V_{storage}} \quad (7)$$

where $N_{H2,storage}$ is the amount of hydrogen in the storage tank [mol] and $V_{storage}$ is the storage volume [m^3].



(**a**) (**b**)

Figure 6. Influence of material properties and physical parameters on hydrogen adsorption isotherms. (**a**) Comparison of three representative adsorbent materials (IRMOF, MSC, and NU) characterized by different bulk densities and pore volumes. (**b**) Sensitivity analysis for IRMOF showing the combined effect of bulk density and pore volume on volumetric hydrogen uptake.

2.3. Techno-Economic Framework

To evaluate the techno-economic performance the system costs need to be calculated. The system costs include capital and operational expenditure for each component (Table 2), where the capital cost for each component are based on the following cost function (8).

$$CAPEX_i = C_{ref} S_{ref} \left(\frac{S_{ref}}{S_{real}}\right)^{-exp} \tag{8}$$

where C_{ref}, S_{ref}, S_{real} and exp are the fitting coefficients [33].

Particular attention is required in the case of hydrogen storage tank cost estimation, where a consistent formulation is needed to allow fair comparison between compressed hydrogen and adsorbent-based configurations. In the extant literature, the financial implications of storage systems are frequently reported in terms of the cost per unit of hydrogen stored. The capital cost of a pressure vessel is determined chiefly by its physical volume and construction material, rather than the actual amount of hydrogen stored. The concept of an equivalent storage volume ($V_{H_2,eq}$) is thus introduced, defined as the product of the physical tank volume and the maximum storage pressure. This definition facilitates consistent cost allocation across disparate storage configurations. In the case of adsorbent-based systems, the cost of the storage material is invoiced separately from the vessel cost. This approach ensures a fair comparison between compressed hydrogen storage and adsorbent-enhanced storage, avoiding distortions that would arise from simply normalising costs by the stored hydrogen mass.

For the compressed hydrogen case, the tank cost is evaluated as in Equation (9).

$$C_{tank} = C_{ref}\, S_{ref} \left(\frac{V_{H_2,eq}}{S_{real}}\right)^{exp} \tag{9}$$

In the physisorption case, the additional contribution of the material is included as in (10).

$$C_{tank,physi} = C_{tank} + C_{material} \cdot V_{tank} \cdot \rho_{bulk} \tag{10}$$

where $C_{material}$ is the material cost in € kg^{-1}.

The capital recovery factor (*CRF*) is utilised to annualise capital expenditures over the component's lifetime, thereby accounting for the time value of money. This approach (11) enables the conversion of the initial financial investment into a uniform annual cost, thereby facilitating consistent comparison across components with differing lifespans, where *n* is the lifetime and i is the discount rate.

$$CRF = \frac{i}{1-(1+i)^{-n}} \tag{11}$$

Operating costs (*OPEX*) are calculated as a percentage of the capital cost of the respective component, including replacement costs if necessary.

The annualised system cost is calculated as in (12):

$$C_{ann} = \left(\sum_i CAPEX_i \cdot CRF + OPEX_i \right) - R \tag{12}$$

where *R* represents the revenues generated from self-consumption incentives, which are calculated as follows in (13).

$$R = C_{TIP} \cdot E_{self-consumption} \tag{13}$$

$E_{self-consumption}$ signifies the total amount of self-produced electricity which is self-consumed by the user. The variable C_{TIP} represents the incentive tariff associated with self-consumption of electricity and is calculated according to Equation (14).

$$C_{TIP} = min[CAP, T_{base} + \max(0; 180 - PZ))] \cdot (1 - FC) \tag{14}$$

Here, *CAP* indicates the maximum incentive tariff limit, which varies according to plant power: 120 € MW^{-1} h^{-1} for plants with power up to 200 kW, 110 € MW^{-1} h^{-1} for plants between 200 kW and 600 kW, and 100 € MW^{-1} h^{-1} for plants with a power output exceeding 600 kW power. T_{base} is the base tariff [€ MW^{-1} h^{-1}] and is defined as follows: 80 € MW^{-1} h^{-1} for plants with power up to 200 kW, 70 € MW^{-1} h^{-1} for plants between 200 kW and 600 kW, 60 € MW^{-1} h^{-1} for plants above 600 kW. *PZ* is the average zonal price [€ MW^{-1} h^{-1}] and it is selected for zone Nord in 2024. *FC* is a correction factor proportional to the percentage of capital contribution, ranging from 0 (no contribution) to 0.5 (a maximum contribution of 40%) [34].

The levelized cost of electricity is calculated as the ratio between the total annualised system costs and the cumulative electricity delivered to the load net of auxiliaries as in Equation (15).

$$LCOE = \frac{C_{ann}}{E_{load}} \tag{15}$$

The optimisation problem is formulated as a multi-objective minimisation problem with the following objective functions (Equations (16) and (17)):

$$f_{obj,A} = \min(C_{ann}) \tag{16}$$

$$f_{obj,B} = \min(E_{grid,buy}) \tag{17}$$

The primary objective is to minimise simultaneously both the total system cost and the electricity purchased from the grid over the entire simulation period. External electricity purchase was chosen as a criterion to encourage greater energy autonomy and aligning with the broader objective of decarbonising energy systems through local, renewable-based self-sufficiency.

The hydrogen storage system is actively engaged in the capture of surplus electricity and the subsequent supply of energy when required. This enhances overall system resilience and contributes to more balanced and dispatchable integration of renewable sources, by mitigating mismatches between generation and demand.

The electricity selling price is conservatively assumed to be zero, with the aim of discouraging the oversizing of on-site generation capacity for the exclusive purpose of exporting surplus energy to the grid. This modelling choice ensures that the optimisation prioritizes local self-consumption and storage integration over economic arbitrage [35,36].

A full-system optimisation is conducted using a multi-objective genetic algorithm (NSGA-III), developed and implemented in a Python-based environment. The simulation model is developed using a rule-based control strategy that prioritizes the use renewable. The NSGA-III algorithm, suitable for high-dimensional, multi-objective problems selects and evaluates each candidate solution. These candidate solutions include a vector of decision variables: the size of the photovoltaic array, the capacities of the electrolyser and fuel cell, and the volume of hydrogen storage. Each variable is explored within a predefined range: PV power capacity from 10 kW to 1 MW, electrolyser and fuel cell sizes from 10 kW to 500 kW, and hydrogen storage volume from 0.01 to 1000 m^3. The NSGA-III algorithm was implemented using the Pymoo Python library with default parameter settings [37]. The algorithm evolves on a population of 150 candidate solutions iteratively, over 100 generations. Variation operators included a simulated binary crossover with a distribution index of 30 and crossover probability of 1.0, and a polynomial mutation with a distribution index of 20. These settings are widely adopted in comparable multi-objective optimisation studies [38], and were chosen as a balanced compromise between convergence quality and computational effort. Given the modest dimensionality of our problem, which involves selecting component sizes, the chosen parameterization (for a total of 15,000 function evaluations) provides sufficient coverage of the search space and is above the typical recommendations found in the literature [39], ensuring both convergence quality

and computational efficiency. The optimisation process continues until the maximum number of generations is reached.

In order to identify a representative solution along the Pareto front, a selection criterion was introduced based on the EU Delegated Acts 2023/1184 and 2023/1185, which define the greenhouse gas emission thresholds for qualifying hydrogen as renewable [40,41]. Specifically, the regulation stipulates a maximum emission limit of 3.34 kg CO_2 per kg of H_2 produced. In consideration of the Italian grid emission factor, which is set at 252 g CO_2 kW^{-1} h^{-1}, this constraint is equivalent to a maximum allowable share of grid electricity of approximately 24% in the total electricity consumed by the hydrogen production system. In order to ensure the maintenance of a conservative buffer, the final selection criterion was set at a maximum grid withdrawal of 20%, thereby ensuring compliance with regulatory frameworks while enabling consistent benchmarking across different configurations.

Table 2. Techno-economic assumptions.

PV		
CAPEX	C_{ref}: 2970 € kW^{-1} S_{ref}: 5 kW exp: 0.91	Extrapolated from [42,43]
OPEX	0.02	[33]
Lifetime	20 y	[33]
PEMEC		
CAPEX	C_{ref}: 1039 € kW^{-1} S_{ref}: 890 kW exp: 0.90	[33]
OPEX	0.07	[33]
Stack replacement time	10 y	[33]
Replacement cost	40%	[33]
Average efficiency	62.5%	[33]
PEMFC		
CAPEX	C_{ref}: 2911€ kW^{-1} S_{ref}:1137 kW exp: 0.92	[33]
OPEX	0.07	[33]
Stack replacement time	10 y	[33]
Replacement cost	40%	[33]
Average efficiency	55%	[33]
H_2 Tank		
CAPEX	C_{ref}: 107 € m^{-3} S_{ref}: 5 m^3 exp: 0.83	Adapted from [33]
OPEX	0.02	[33]
Storage material	3.5–35 € kg^{-1}	[18,19]
Lifetime	20 y	[33]
Compressor		
CAPEX	C_{ref}: 1769 € kW^{-1} S_{ref}: 2154 kW exp: 0.77	[33]
OPEX	0.07	[33]
Replacement time	15 y	[33]
Efficiency	71%	[33]
General		
Discount rate	5%	[36]
Grid price	PUN(2024) ·1.7	[22,23]
Project lifetime	20 y	[33]

3. Results

The outcome of each simulation encompasses detailed time-resolved profiles of power flows between the photovoltaic array, electrolyser, hydrogen storage tank, proton exchange membrane fuel cell, community load, and the external grid. These time series reveal the dynamic operation of the Power-to-Power system under realistic annual boundary conditions.

Complementing the temporal data, a comprehensive set of annual performance indicators is presented, derived through a multi-objective optimisation framework. An analysis of the levelized cost of electricity is conducted as a function of both the cost and intrinsic properties of the hydrogen storage material, specifically bulk density and pore volume, enabling assessment of techno-economic impacts tied to different adsorbent characteristics.

The dynamic behaviour of the storage tank is further explored through the evolution of its state-of-charge over time, which reveals diverse operational regimes ranging from daily or sub-monthly cycling to long-term seasonal buffering. In addition, the variation of average storage pressure as a function of tank volume is analysed to evaluate the interplay between material properties, storage capacity, and operating conditions. This relationship is crucial for identifying optimal system configurations that minimise compression energy losses while maintaining performance targets.

Finally, a Sankey diagram is employed to visualise energy conversion and distribution pathways within the system, illustrating both electrical and thermal interactions among components. This integrative presentation supports a holistic understanding of system sizing, performance trade-offs, and the role of hydrogen storage properties in achieving efficient, robust, and economically viable P2P operation.

Figure 7 displays a Pareto front resulting from the multi-objective optimisation process, which captures the trade-off between the levelized cost of electricity and the share of electricity withdrawn from the grid. A clear inverse relationship emerges: as grid dependency increases, system costs decrease, reflecting the reduced need for oversized system components. At high levels of external electricity supply, the system can operate with minimal investment in generation and storage infrastructure, thereby limiting capital expenditures and mitigating conversion losses associated with hydrogen pathways.

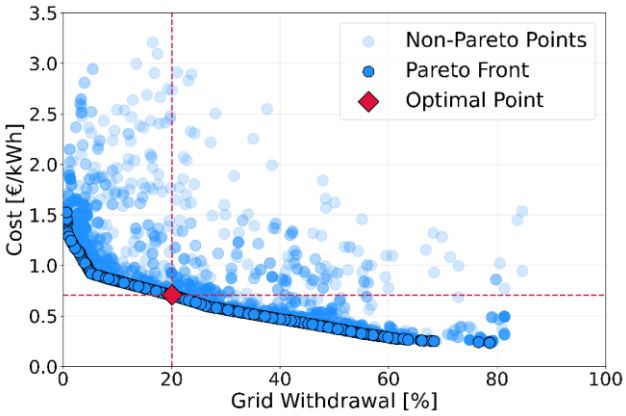


Figure 7. Pareto front showing the trade-off between LCOE and the share of electricity withdrawn from the grid. The selected optimal configuration, highlighted in red, corresponds to a grid withdrawal of 20%, in alignment with regulatory emission thresholds.

However, as the grid withdrawal is progressively reduced, moving towards higher degrees of energy autonomy, the total system cost rises sharply. This trend is particularly pronounced below 5% grid dependency, where the LCOE can exceed 1.5 € kW^{-1} h^{-1}. In this regime, the system must compensate for prolonged periods of low renewable generation, which necessitates significant over-dimensioning of both the photovoltaic array and the hydrogen-based storage infrastructure.

Beyond approximately 60% grid withdrawal, further increases in external electricity supply have only a minor effect on LCOE. In this domain, the role of hydrogen storage becomes marginal, as the energy system relies primarily on direct supply from the grid and the remaining part is covered directly by PV electricity. This reduces the need for investment in electrolysers, fuel cells, and storage tanks, and avoids the round-trip efficiency losses intrinsic to hydrogen conversion. The overall shape of the Pareto front thus reflects the interplay between energy autonomy and economic viability, providing a comprehensive view of the optimisation landscape.

3.1. Sensitivity Regarding Storage Material and Cost

Figure 8 presents the results of the LCOE sensitivity analysis, with the left panel showing variations associated with bulk density and pore volume for IRMOF-1 at a fixed material cost of 3.5 € kg^{-1}, and the right panel illustrating the impact of material cost for three representative adsorbents.

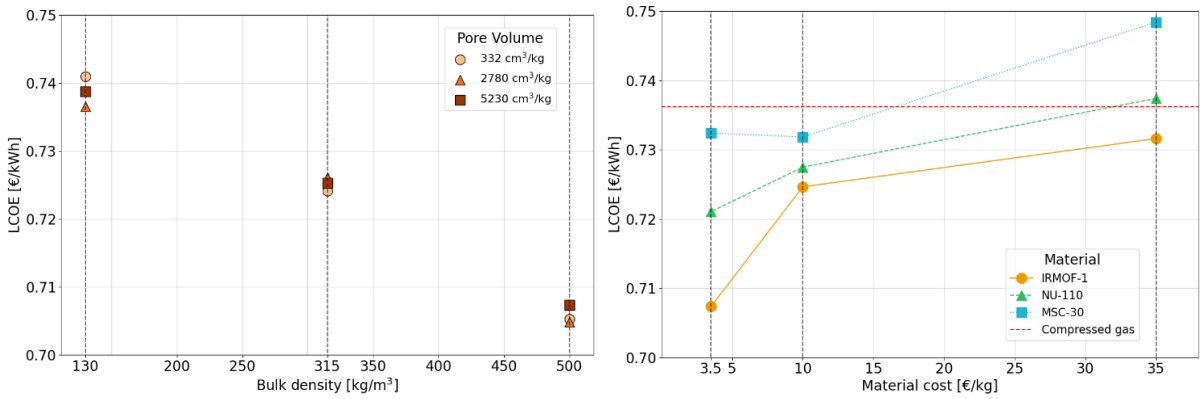


Figure 8. Optimized LCOE for different bulk densities and pore volume using IRMOF as a material and 3.5 € $kg^{-1}_{material}$ (**left**). Optimized LCOE as a function of material cost (**right**).

For IRMOF-1 (left), the analysis reveals that bulk density is much more impactful than the pore volume parameter. An increase from 130 to 500 kg m^{-3} yields a reduction in the levelized cost of electricity from 0.741 to 0.705 € kW^{-1} h^{-1}, corresponding to a relative decrease of approximately 4.9%**.** In contrast, pore volume shows a minimal influence: varying it from 332 cm^3 kg^{-1} to 5230 cm^3 kg^{-1} at fixed bulk density leads to LCOE changes of less than 0.3%**.** This slight variation may be attributed to the inherent variability of the heuristic optimisation algorithm rather than a direct causal effect of pore volume, as no clear or monotonic trend between LCOE and pore volume is observed. This confirms that, under ambient temperature conditions, higher packing density is far more critical than maximizing porosity when aiming to reduce system-level costs.

The right panel of Figure 8 examines the sensitivity of LCOE to the material cost for IRMOF-1, NU-110, and MSC-30. At lower costs (3.5 € kg^{-1}), IRMOF-1 yields the most competitive LCOE at 0.707 € kW^{-1} h^{-1}, followed by NU-110 at 0.721 € kW^{-1} h^{-1} and MSC-30 at 0.732 € kW^{-1} h^{-1}. As material costs increase to 35 € kg^{-1}, the LCOE rises accordingly, but at different rates. IRMOF-1 remains the most cost-effective option (0.732 € kW^{-1} h^{-1}), while MSC-30 reaches the highest value (0.748 € kW^{-1} h^{-1}), primarily due to its lower hydrogen uptake performance and the resulting increase in required storage volume.

A red dashed line in the graph indicates the LCOE associated with a reference compressed hydrogen system (0.736 € kW^{-1} h^{-1}). Notably, IRMOF-1 and NU-110 outperform the compressed gas benchmark up to material costs around 30 € kg^{-1}, highlighting their potential in practical applications if material production costs can be sufficiently low. It should also be noted, however, that the assumed cost of 3.5 € kg^{-1} is currently more realistic for activated carbons such as MSC-30, while it remains a highly ambitious target for metal-organic frameworks. This underscores the importance of ongoing efforts to reduce MOF synthesis costs if these materials are to be deployed competitively in large-scale energy storage systems.

3.2. Storage Influence on System Behaviour

Figure 9 presents the sensitivity analysis of the optimized hydrogen storage capacity, first as a function of bulk density and pore volume for IRMOF-1 (left), and then as a function of material cost for different adsorbents (right).

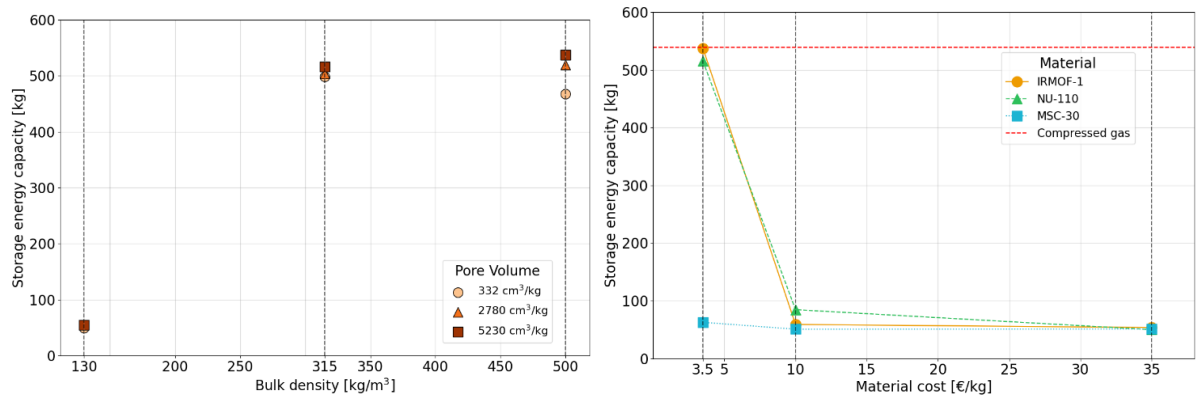


Figure 9. Optimized hydrogen storage capacity for different bulk densities and pore volume using IRMOF as a material and 3.5 € $kg^{-1}_{material}$ (**left**). Optimized hydrogen storage capacity as a function of material cost (**right**).

In the case of IRMOF-1, the analysis confirms that bulk density is the dominant parameter influencing total hydrogen storage capacity. The bulk density has been tested as sensitivity across the range 130–500 kg m^{-3}. Increasing the bulk density from 130 to 315 kg m^{-3} results in a more than tenfold increase in stored hydrogen mass, from approximately 50 kg to over 500 kg, under identical material cost assumptions. A further increase to 500 kg m^{-3} leads only to a marginal additional gain (up to 537 kg), indicating that above a certain threshold, bulk density improvements yield diminishing returns in terms of usable storage capacity. This saturation effect is not due to material limitations but rather reflects system-level constraints. Once the tank is dimensioned to support seasonal long-duration energy balancing, further capacity becomes underutilised.

Pore volume, in contrast, exhibits only a minor influence on storage capacity. For each bulk density level, varying the pore volume across the tested range (332–5230 cm^3 kg^{-1}) results in capacity changes of less than 4%, with no clear trend. These small variations might be related due to interactions between design variables within the optimisation algorithm, rather than a direct impact of porosity itself. This reinforces the conclusion that packing density, rather than internal surface area, is the key driver of system-level hydrogen storage performance under ambient conditions.

The right panel of Figure 9 compares the maximum hydrogen storage capacity achieved as a function of material cost for IRMOF-1, NU-110, and MSC-30. When all materials are assumed to cost 3.5 € kg^{-1}, IRMOF-1 achieves the highest capacity (537 kg), followed closely by NU-110 (515 kg), while MSC-30 lags behind with only 63 kg due to its lower bulk density and hydrogen uptake. As material costs increase to 35 € kg^{-1}, storage capacities drop significantly across all materials, particularly for IRMOF-1 (53.7 kg) and NU-110 (50.1 kg), due to cost-driven constraints on tank volume. Interestingly, MSC-30 shows relatively stable capacity regardless of cost, suggesting that its performance is strongly limited by material properties. Notably, at the lowest cost scenario (3.5 € kg^{-1}), both IRMOF-1 and NU-110 reach storage capacities that are comparable to the benchmark provided by compressed hydrogen storage (indicated by the red dashed line), highlighting their potential viability as alternative storage media under favourable economic conditions.

These sizing differences have direct implications for the system's operation: depending on the selected storage capacity, the hydrogen tank supports either long-duration seasonal balancing or short-term cycling. This contrast is clearly reflected in the state-of-charge profiles shown in Figure 10, which illustrate the system's behaviour across the full simulation year for two representative configurations.

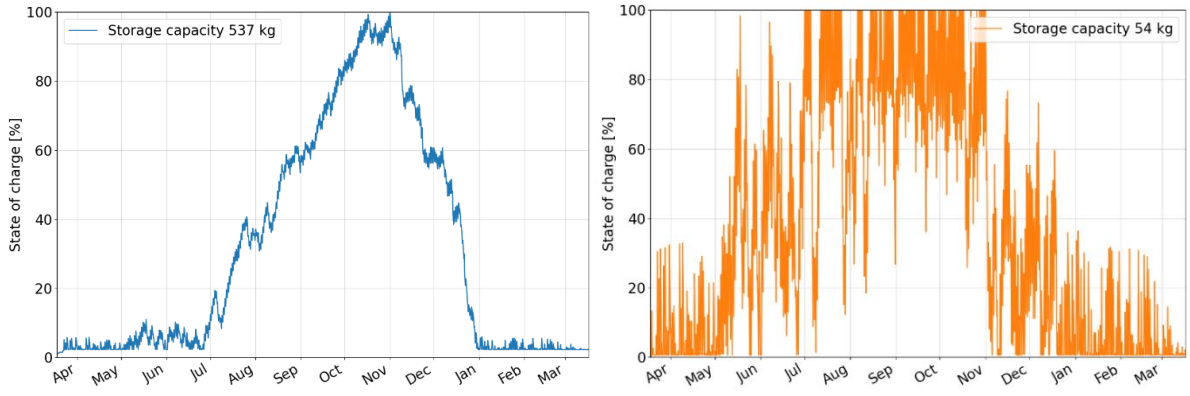


Figure 10. Annual state-of-charge (SOC) profiles for hydrogen storage under two different capacity configurations using IRMOF-1: 537 kg (3.5 € kg^{-1}) and 54 kg (35 € kg^{-1}).

At low material cost (3.5 € kg^{-1}), the system is able to deploy a high-capacity tank (537 kg), enabling a seasonal storage regime (9–10 full cycles per year). Hydrogen is gradually accumulated from late spring to mid-autumn, reaching full saturation around October, and is subsequently discharged throughout the winter. This configuration allows long-duration energy balancing and corresponds to the upper bound of useful capacity for the given energy demand and renewable generation profile.

Conversely, when the material cost rises to 35 € kg^{-1}, the storage capacity is reduced to approximately 54 kg. Under this constraint, the system operates in a short-term cycling mode (80–100 full cycles per year), with frequent daily charge and discharge events driven by the mismatch between solar generation and load. While the SOC shows high-frequency variability, it also retains a weaker seasonal component: storage levels tend to be higher during summer months and progressively decrease during winter, indicating that, even at reduced capacity, the system maintains some ability to shift energy over longer timescales. This hybrid behaviour reflects the system's effort to maximise the utility of limited storage volume. Together, these two cases illustrate the dual operational

roles of hydrogen storage: either as a seasonal energy buffer under favourable techno-economic conditions, or as a short-term balancing tool in cost-constrained scenarios.

The implications of material selection and adsorbent properties extend beyond storage capacity to influence key design parameters such as tank volume and operating pressure. Figure 11 illustrates the relationship between these two variables for both IRMOF-1, with varying bulk densities and pore volumes), and for the three materials considered at different cost levels.

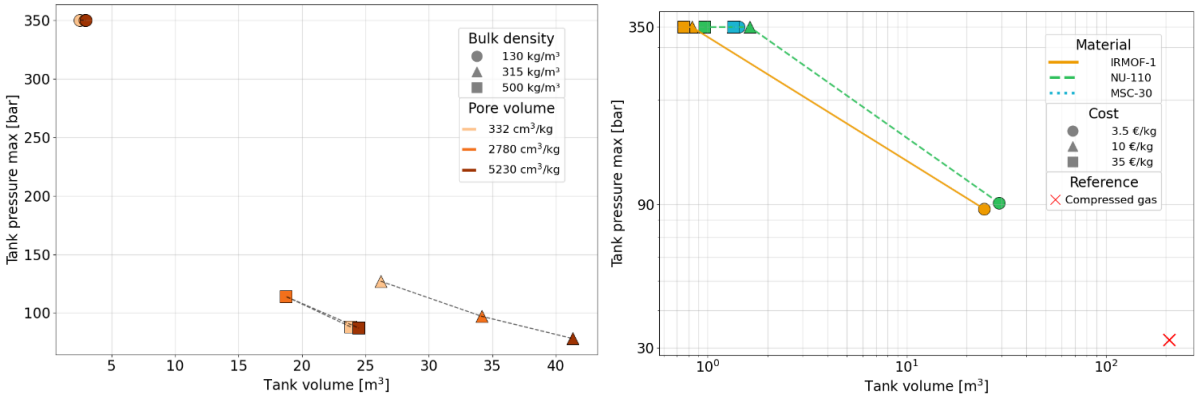


Figure 11. Tank pressure vs. tank volume for different bulk densities and pore volume using IRMOF as a material and 3.5 € $kg^{-1}_{material}$ (**left**). Tank pressure vs. volume for different materials and cost scenarios (**right**).

In the case of IRMOF-1 (left panel), increasing bulk density leads to a notable reduction in the required storage pressure. At 130 kg m^{-3}, the system reaches the upper operational pressure limit (350 bar) regardless of pore volume, due to the low volumetric hydrogen uptake. As bulk density increases, the system can achieve the same energy storage target at much lower pressures, down to around 78–127 bar depending on pore volume. In parallel, tank volume increases with decreasing bulk density, ranging from less than 3 m^3 at 130 kg m^{-3} to over 40 m^3 at 315 kg m^{-3}. This inverse correlation reflects a fundamental design trade-off. While lower bulk densities require higher pressures and enable smaller tanks, this configuration is only favourable when the additional compression cost, including both capital and operational expenses, is more economical than increasing the quantity of adsorbent material. Conversely, at higher bulk densities, the system can afford larger tank volumes at lower pressures, making it preferable to invest in tank capacity rather than in compression infrastructure or more expensive operation.

Pore volume also has a secondary influence on these trends. For a given bulk density, higher pore volumes slightly increase the storage volume but often allow a reduction in operating pressure. This effect is particularly visible at 315 and 500 kg m^{-3}, where pressure varies between 78 and 127 bar depending on the internal porosity. Nonetheless, bulk density remains the dominant parameter in determining both pressure and volume requirements.

The right panel of Figure 11 extends the analysis to a cost-based comparison between materials. At high material costs (35 € kg^{-1}), the system opts for minimal tank volumes (under 1.5 m^3), but the low storage capacity forces operation at the upper design pressure of 350 bar for all materials. This pressure ceiling represents not only a mechanical design constraint but also a point of diminishing economic return, as it imposes additional requirements on tank integrity, safety systems, and compression energy. In contrast, at lower costs (3.5 € kg^{-1}), materials like IRMOF-1 and NU-110 enable significantly larger storage volumes (24–29 m^3), while operating at much lower pressures (87–91 bar), resulting in more balanced and efficient system configurations. MSC-30 remains pressure-constrained even at low cost due to its limited volumetric performance. The compressed gas configuration, represented by the red cross, relies on considerably larger storage volumes (over 200 m^3) but operates at much lower pressures (30 bar). This configuration becomes economically favourable in the absence of material costs, as the expense of scaling up tank volume is outweighed by the significant savings from avoiding both the purchase and operation of a compression unit.

These findings highlight the triangular relationship between material properties, cost assumptions, and system-level design choices. High-performance materials with favourable bulk densities enable large tank volumes and low operating pressures, which in turn reduce parasitic energy demand and improve overall system efficiency. Conversely, when the system is constrained to operate near the 350 bar threshold, compression power increases significantly, with annual electricity consumption by the compressor reaching up to 4.4 MW h per year in the worst-case configuration (130 kg m^{-3}, high pressure). In contrast, optimised low-pressure systems such as IRMOF-

1 at 87 bar require only 1 MW h per year. These auxiliary loads are reflected qualitatively in the LCOE trends discussed in Section 3.2, where lower-pressure configurations tend to achieve better cost performance, despite higher upfront material costs, thanks to improved round-trip efficiency and reduced operational losses.

The Sankey diagrams in Figure 12 compare the full energy balances of the system under two distinct material cost scenarios. The structure and routing of the energy flows change significantly, depending on the storage capacity and its interaction with the other components. All flow percentages are expressed relative to the total renewable energy production.

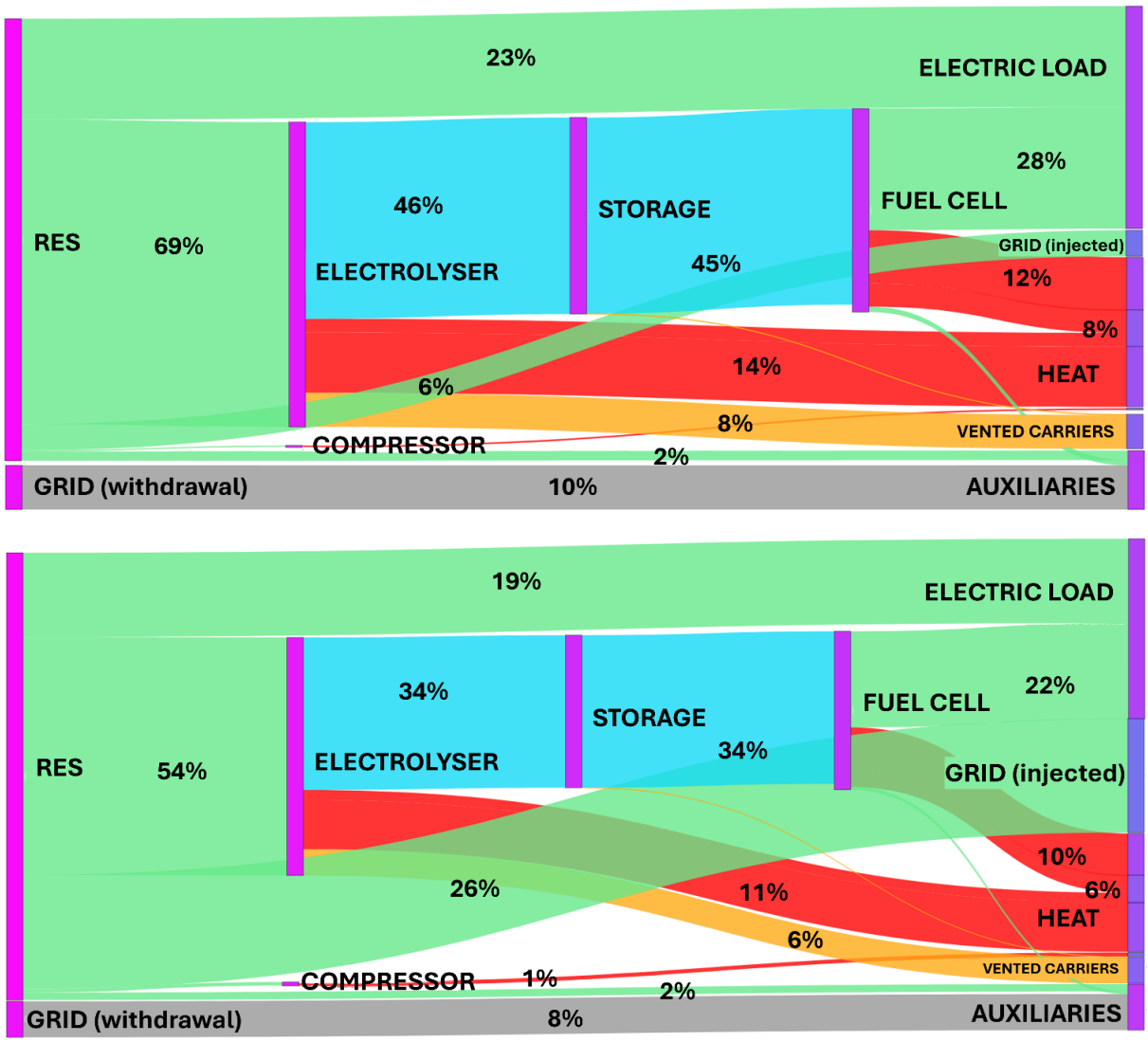


Figure 12. Annual energy flow diagrams for the optimized P2P system using IRMOF-1 as storage material at two cost scenarios: 3.5 € kg^{-1} (**top**) and 35 € kg^{-1} (**bottom**).

At a low material cost (3.5 € kg^{-1}), the system installs a large hydrogen storage volume, to reach the 80% self-sufficiency requirement. In this case, approximately 25% of the total renewable electricity is consumed directly to meet the electric load, while an additional 69% is directed to the hydrogen storage pathway. Specifically, this share is processed by the electrolyser, which converts 46% of the incoming RES into hydrogen. The stored hydrogen is then reconverted into electricity via the fuel cell, which returns 28% of the total RES to the load. This corresponds to an overall round-trip electrical efficiency of about 40% for the EL–storage–FC loop. Only 6% of the renewable generation is exported to the grid. Due to improved material performance, lower storage pressures are sufficient, making the compressor's electricity consumption negligible (0.2%). As illustrated in Figure 12, the 20% grid withdrawal—equivalent to a 10% RES share—is allocated exclusively to covering auxiliary loads. The remaining renewable energy is mostly dissipated in form of low- to medium-temperature heat (80 °C), due to conversion losses on the hydrogen pathway, part of which could be potentially recovered in integrated thermal applications (e.g., space heating, domestic hot water).

At a high material cost (35 € kg^{-1}), the system is forced to reduce the storage capacity significantly, leading to a less efficient overall configuration. Only 21% of the RES is directly consumed, and 54% is processed via storage, lower than in the previous case. The grid injection increases notably to 26%**,** indicating a surplus of unutilized energy due to the limited capacity of the hydrogen pathway. The compressor accounts for a small, but non-negligible fraction (1.5%) of RES consumption, as higher pressures are required to compensate for the lower material density. In this scenario, 34% of the total renewable electricity is converted into hydrogen by the electrolyser, and 22% is subsequently recovered as electricity by the fuel cell. While the overall round-trip through storage is less efficient, the system still retains a high level of renewable utilization, albeit with increased external reliance for auxiliary functions. In both cases, the grid is never used to feed the electrolyser or storage, but only to power the auxiliary loads.

Beyond energy flows, the two configurations differ significantly in terms of component sizing and annual energy production. At low material cost (3.5 € kg^{-1}), the system favours a larger fuel cell (102 kW) and electrolyser (161 kW), paired with a moderate PV array (299 kW). This sizing ensures a higher storage turnover and allows for efficient cycling at lower pressures (87 bar). Despite the smaller PV installation, the annual RES production remains high (380 MW h), and the total amount of hydrogen stored reaches over 537 kg, thanks to the large tank volume (24.5 m^3) and favourable material properties.

At high material cost (35 € kg^{-1}), the system requires a larger PV plant (374 kW) to compensate for the reduced storage flexibility. The electrolyser and fuel cell are smaller (146 and 97 kW, respectively), reflecting the limited size of the hydrogen pathway (only 53.7 kg stored at 350 bar in 0.76 m^3). Consequently, a higher share of electricity is either curtailed (122 MW h not used) or injected into the grid, reducing the overall system efficiency. Compressor electricity consumption also increases significantly (up to 3.86 MW h per year), further reducing net performance.

These results underline the non-linear trade-off between material cost and system design. At low cost, the system leverages storage capacity to reduce oversizing of generation, whereas at high cost, it relies more on PV and grid injection to manage intermittency. The LCOE difference, 0.707 vs. 0.731 € kW^{-1} h^{-1}, captures not only investment shifts, but also the cumulative effect of these operational dynamics.

4. Discussion

The results of this study provide a detailed picture of the complex trade-offs underlying the techno-economic performance of Power-to-Power systems based on ambient-temperature hydrogen storage via physisorption. Despite the relatively high levelized cost of electricity obtained in several configurations, particularly under low grid withdrawal conditions, certain system setups already approach or even meet international cost targets, pointing to specific pathways for improvement and deployment.

In order to establish a baseline for comparison, the hydrogen storage system was first modelled considering only compressed hydrogen, without the addition of adsorbent materials. Within the multi-objective optimisation framework, this configuration is not treated as a simple benchmark but is optimised consistently with the other scenarios, ensuring that photovoltaic sizing, electrolyser and fuel cell capacities, and storage volume are adjusted to minimise costs and grid dependency. The resulting performance indicators are broadly consistent with trends reported in the literature for compressed hydrogen storage systems. This general agreement lends support to the robustness of the modelling approach and suggests that the optimisation procedure yields plausible results. In particular, Marocco et al. [44] analysed a P2P system with a PEM electrolyser of comparable scale, reporting an LCOE of 0.844 € kW^{-1} h^{-1}. This value is in close agreement with the result obtained here for the compressed-hydrogen-only scenario (0.736 € kW^{-1} h^{-1}), despite their system employing a storage capacity that is nearly half the size of that identified as optimal in the present optimisation framework. Such consistency reinforces the reliability of the model and confirms that the compressed hydrogen case represents a credible and comparable reference point for subsequent evaluations.

The integration of physisorption materials within the storage system facilitates a comparative evaluation of the advantages associated with adsorbent-based storage methods. In comparison with the work of Minuto et al. [16] which evaluates material performance without system-level optimisation, the results of this study emphasise the value of integrating material parameters into a techno-economic optimisation framework. Specifically, while Minuto et al. demonstrate the potential of adsorbents to reduce storage pressure up to 70–80% and modestly improve round-trip efficiency, our optimised scenarios reveal how these material-level improvements translate into more competitive system-level performance. The comparison demonstrates that, under optimisation, the incorporation of physisorption materials not only provides enhanced volumetric capacity but also improves system cost-effectiveness when benchmarked against conventional compressed hydrogen storage.

One of the main outcomes concerns the strong sensitivity of the system to the adsorbent material's bulk density. Across all simulations, bulk density proved to be the dominant physical parameter affecting both the optimal storage capacity and the system-wide LCOE. Higher bulk density enables more hydrogen to be stored at a given volume and pressure, ultimately reducing the tank size and, more importantly, lowering compression energy demand and auxiliary power consumption. This behaviour aligns with adsorption isotherm trends and highlights the practical advantage of increasing material packing over simply maximizing surface area. On the contrary, pore volume exhibited only a marginal effect on both storage performance and economic indicators, especially within the operating conditions considered here. These results are in line with the findings of Minuto et al. [16], who likewise identified bulk density as the decisive property determining whether adsorbents outperform or underperform compressed hydrogen storage, confirming the central role of densification in achieving practical benefits. Material development efforts should therefore prioritise densification strategies rather than porosity enhancement when targeting ambient temperature storage applications.

The assumed cost of 3.5 € kg^{-1} was used as a baseline to evaluate material performance under equal economic assumptions. At this level, IRMOF-1 with bulk densities of 315 kg m^{-3} and above, achieved specific storage costs in the range of 6.76–9.51 € kW^{-1} h^{-1}, thereby complying with the U.S. Department of Energy (DOE) target of 10 \$ kW^{-1} h^{-1} for hydrogen storage systems in vehicles [20]. Notably, this cost level is already realistic for activated carbons such as MSC-30 [45], but remains aspirational for more advanced MOFs like IRMOF-1 and NU-110, whose synthesis costs currently range between 35 and 70 € kg^{-1} [18]. Peng et al. [19] sets a target production cost for MOFs around 10 \$ kg^{-1}, which would represent a significant step toward economic viability for large-scale energy storage applications.

A closer look at the storage cost (€ kW^{-1} h^{-1} values) obtained across all scenarios reinforces this conclusion. IRMOF-1 meets the DOE threshold not only at 3.5 € kg^{-1} and high bulk densities, but also at a material cost of 10 € kg^{-1}, provided the bulk density reaches 500 kg m^{-3} and the pore volume is high. NU-110 also achieves compliance at 3.5 € kg^{-1}, with values around 8.87 € kW^{-1} h^{-1}. Conversely, all other combinations of material cost and physical properties fall short of this benchmark. MSC-30, in particular, exceeds 15 € kW^{-1} h^{-1} even at 3.5 € kg^{-1}, reaching up to 33.5 € kW^{-1} h^{-1} at higher cost assumptions, well above feasible thresholds for large-scale deployment.

A useful comparison can be drawn with the recent study by Peng et al. [19], which reports levelized costs of storage (LCOS) below 5 € kW^{-1} h^{-1} for MOF-based systems operated at moderately reduced temperatures (223 K) and elevated pressures (up to 170 bar). In the optimisation framework employed, there is attainment of analogous values in certain scenarios; however, the LCOS exhibits an ascent above this threshold in instances of elevated material costs, thereby underscoring the prevailing significance of adsorbent cost in both analyses. The primary distinction between the two lies in their operational conditions: while the outcomes of the former are enhanced by increased uptake at sub-ambient temperatures, this is accompanied by an increase in system complexity for thermal management. In contrast, the present study focuses on ambient-temperature operation, where cost competitiveness is primarily determined by material densification and synthesis cost reduction. The findings of both studies indicate that material cost and operating conditions are pivotal in the advancement of MOF-based hydrogen storage. The results demonstrate that a target cost of 5 € kW^{-1} h^{-1} can be attained even under ambient conditions, provided that favourable material properties are coupled with system-level optimisation. While this threshold is not reached in the present study, specific storage costs as low as 6.76 € kW^{-1} h^{-1} were achieved, indicating promising potential for further improvements through material and process optimisation.

The broader system-level implications of these trends are significant. Material properties and cost directly influence tank size, operating pressure, and auxiliary energy consumption. When the system is forced to operate near the design pressure ceiling of 350 bar, as in many of the cost-constrained scenarios, compressor electricity demand becomes substantial, reaching up to 4.4 MW h per year. In contrast, configurations operating at lower pressures (e.g., 87-127 bar) consume less than 1.5 4 MW h per year for compression. These auxiliary demands are reflected in the LCOE results and further justify the selection of materials that enable operation at reduced pressure.

Although the overall LCOE values remain above typical electricity retail prices, especially in highly autonomous configurations, such systems may still find strategic relevance in remote or off-grid contexts. Here, the value of energy independence, especially when replacing diesel generation, can offset the higher upfront and operational costs. Moreover, the capability of hydrogen storage to support seasonal energy shifting, as demonstrated in the SOC profiles, positions it as a compelling solution for locations with pronounced solar intermittency.

In terms of scalability, the ability of the system to adapt its operation across a wide range of capacities, from daily cycling to seasonal buffering, demonstrates its flexibility. However, further work is needed to assess long-term durability, thermal integration options (e.g., low-grade heat recovery), and hybridisation with short-duration storage technologies like batteries. The current study also assumes ambient temperature operation, but the

introduction of cooling systems or operation under cryogenic conditions (e.g., at 77 K) may further improve storage density, albeit at the cost of additional thermal management complexity.

Despite the geographical focus of the case study on Northern Italy, the conclusions of this work are not geographically constrained. The modelling framework is fully parametric, and input datasets such as solar irradiance, demand profiles, grid carbon intensity, and electricity prices can be readily substituted with those of other regions. While the absolute results, for example, the LCOE or the optimal sizing of photovoltaic capacity, will vary with local solar availability and market conditions, the broader trends identified remain valid. In particular, the critical influence of bulk density on storage performance, the relative marginality of pore volume, and the comparative behaviour of compressed versus adsorbent-based storage hold across different contexts. This finding suggests that the framework can be applied to assess techno-economic feasibility in a range of geographical and regulatory settings.

The dynamic simulation is conducted over a one-year period, with performance assumed constant, while the long-term ageing effects are incorporated at the techno-economic level, through operational expenditures and stack replacement costs over the 20-year project lifetime. This methodological approach ensures that the financial implications of degradation are included in the LCOE, while avoiding additional complexity in the performance model. The integration of degradation models into the optimisation framework could be explored in future work, as it may help capture efficiency decay more explicitly and provide a more comprehensive evaluation of its impact on system performance and costs.

In addition, the hydrogen storage block is based on a previously published work by Rozzi et al. [17]. In that study the adsorption/desorption thermodynamics of the adsorbent bed were not modelled, since at room temperature the heat effects involved are relatively small (enthalpy of adsorption in the range of 4–10 kJ mol^{-1}) and can be dissipated or absorbed by the environment due to the high thermalisation of hydrogen. Consequently, the thermal management of the adsorbent bed was deemed negligible, and the tank was treated under isothermal conditions. The development of a comprehensive thermal management model would necessitate the acquisition of detailed adsorption enthalpy data at varying coverages and high-pressure calorimetric measurements. However, these data are not readily available in the extant literature.

Finally, future research should incorporate more comprehensive techno-economic frameworks including incentive mechanisms, and carbon taxation. This would allow a better assessment of when and where hydrogen-based P2P systems may become competitive with other decarbonisation pathways. Such analysis would also clarify the role of hydrogen storage in the broader context of resilient and low-carbon energy systems.

5. Conclusions

This study has presented a techno-economic analysis of a Power-to-Power system integrating photovoltaic generation with hydrogen-based seasonal storage, employing adsorptive hydrogen storage materials. Through multi-objective optimisation, we evaluated the trade-offs between system cost and grid dependency, identifying a reference operating point with 20% grid withdrawal, consistent with current decarbonisation targets.

The results show that, although LCOE values remain high compared to conventional energy sources, rising above 1.5 € kW^{-1} h^{-1} under low grid reliance, the system becomes increasingly competitive in remote or off-grid contexts, where alternatives are limited and energy autonomy is critical. In such cases, the strategic benefits of local energy independence may outweigh the higher investment costs.

A comparison with the baseline case of compressed hydrogen storage reveals that the potential of utilisation of adsorbent materials for enhancing storage capacity under favourable conditions. At low material costs (3.5 € kg^{-1}), IRMOF-1 and NU-110 achieve maximum storage capacities of 537 kg and 515 kg, respectively, values that are directly comparable to those obtained with compressed hydrogen alone. This finding suggests that, under conditions of sufficiently high bulk density and moderate cost constraints, adsorbents have the capacity to match the established benchmark while concurrently facilitating reduced operating pressures and decreased compressor electricity demand. Conversely, activated carbon MSC-30 maintains a consistently lower position in comparison to the compressed hydrogen reference, a consequence of its constrained bulk density and capacity for uptake. This finding indicates that, in the context of large-scale seasonal storage, advanced MOFs have the potential to offer performance comparable to that of conventional compressed storage. Additionally, they offer the advantage of enhanced system efficiency and safer, lower-pressure operation, provided that synthesis costs are reduced towards the projected targets.

The analysis confirms that bulk density is the most influential adsorbent property in determining both storage capacity and system-level performance. A transition from 130 to 500 kg m^{-3} enables over tenfold increases in stored hydrogen mass and allows operation at significantly lower pressures. Conversely, pore volume has limited

impact on performance, suggesting that material research should prioritise densification over surface area maximization under ambient temperature conditions.

While the assumed adsorbent cost of 3.5 € kg^{-1} permits advantageous configurations, particularly with IRMOF-1 and NU-110, only a subset of these scenarios achieve compliance with the U.S. DOE storage cost target of 10 \$ kW^{-1} h^{-1}. Specifically, IRMOF-1 with high bulk density (≥315 kg m^{-3}) and low material cost (≤10 € kg^{-1}), or NU-110 at 3.5 € kg^{-1}, remain within this threshold. Other materials or cost conditions, especially MSC-30, despite its commercial viability, struggle to meet this criterion due to lower volumetric performance.

The operational role of hydrogen storage emerges as dual: enabling seasonal balancing under favourable economic conditions, or short-term buffering when material cost imposes stricter design constraints. This flexibility highlights hydrogen's unique potential in energy systems characterized by long-term mismatches between supply and demand.

Beyond materials, storage pressure and compression energy demand are shown to significantly affect auxiliary loads and indirectly impact LCOE.

Policy implications arise from these findings: to make P2P hydrogen systems viable at scale, a combination of material innovation, manufacturing cost reduction, and support mechanisms (e.g., capital incentives, carbon pricing, or regulatory targets) will be necessary. The scalability of adsorptive hydrogen storage is promising, but its widespread deployment will depend on aligning technological potential with economic feasibility and policy frameworks.

Author Contributions

E.M.: methodology, writing-original draft preparation, investigation; M.S.: conceptualization, methodology, writing-reviewing and editing, investigation; E.R.: conceptualization, methodology, writing-original draft preparation, software, investigation; F.D.M.: conceptualization, methodology, supervision, writing-reviewing and editing; A.L: conceptualization, methodology, supervision, writing-reviewing and editing. All authors have read and agreed to the published version of the manuscript.

Funding

This study was carried out as part of the National Recovery and Resilience Plan (PNRR) and received funding from the Italian Ministry of the Environment and Energy Security, for the "Novel Materials for Hydrogen storage (NoMaH)" project, ID RSH2A_000035, CUP: F27G22000180006.

This manuscript only reflects the authors' views and opinions, and neither the European Union nor the European Commission can be considered responsible for them.

Data Availability Statement

No new data were generated for this study. All data supporting the findings of this work are openly available in the cited references and properly acknowledged in the text.

Conflicts of Interest

The authors declare that they have no known competing financial interests or personal relationships that could have appeared to influence the work reported in this paper.

References

1. *Net Zero by 2050—A Roadmap for the Global Energy Sector*; IEA: Singapore, 2021.
2. World Energy Outlook 2024—Analysis Available online: https://www.iea.org/reports/world-energy-outlook-2024 (accessed on 1 July 2025).
3. Suraparaju, S.K.; Samykano, M.; Vennapusa, J.R.; et al. Challenges and Prospectives of Energy Storage Integration in Renewable Energy Systems for Net Zero Transition. *J. Energy Storage* **2025**, *125*, 116923. https://doi.org/10.1016/j.est.2025.116923.
4. Worku, M.Y. Recent Advances in Energy Storage Systems for Renewable Source Grid Integration: A Comprehensive Review. *Sustainability* **2022**, *14*, 5985. https://doi.org/10.3390/su14105985.
5. Volfkovich, Y.M. Electrochemical Supercapacitors (a Review). *Russ. J. Electrochem.* **2021**, *57*, 311–347. https://doi.org/10.1134/S1023193521040108.

6. Ursua, A.; Gandia, L.M.; Sanchis, P. Hydrogen Production from Water Electrolysis: Current Status and Future Trends. *Proc. IEEE* **2012**, *100*, 410–426. https://doi.org/10.1109/JPROC.2011.2156750.
7. Bhandari, R.; Adhikari, N. A Comprehensive Review on the Role of Hydrogen in Renewable Energy Systems. *Int. J. Hydrogen Energy* **2024**, *82*, 923–951. https://doi.org/10.1016/j.ijhydene.2024.08.004.
8. Barthelemy, H.; Weber, M.; Barbier, F. Hydrogen Storage: Recent Improvements and Industrial Perspectives. *Int. J. Hydrogen Energy* **2017**, *42*, 7254–7262. https://doi.org/10.1016/j.ijhydene.2016.03.178.
9. Muthukumar, P.; Kumar, A.; Afzal, M.; et al. Review on Large-Scale Hydrogen Storage Systems for Better Sustainability. *Int. J. Hydrogen Energy* **2023**, *48*, 33223–33259. https://doi.org/10.1016/j.ijhydene.2023.04.304.
10. Zhang, L.; Allendorf, M.D.; Balderas-Xicohténcatl, R.; et al. Fundamentals of Hydrogen Storage in Nanoporous Materials. *Prog. Energy* **2022**, *4*, 042013. https://doi.org/10.1088/2516-1083/ac8d44.
11. Hirscher, M.; Zhang, L.; Oh, H. Nanoporous Adsorbents for Hydrogen Storage. *Appl. Phys. A* **2023**, *129*, 112. https://doi.org/10.1007/s00339-023-06397-4.
12. Klopčič, N.; Grimmer, I.; Winkler, F.; et al. A Review on Metal Hydride Materials for Hydrogen Storage. *J. Energy Storage* **2023**, *72*, 108456. https://doi.org/10.1016/j.est.2023.108456.
13. Kilic, M.; Altun, A.F. Dynamic Modelling and Multi-Objective Optimization of off-Grid Hybrid Energy Systems by Using Battery or Hydrogen Storage for Different Climates. *Int. J. Hydrogen Energy* **2023**, *48*, 22834–22854. https://doi.org/10.1016/j.ijhydene.2022.12.103.
14. Li, J.; Li, G.; Ma, S.; et al. Modeling and Simulation of Hydrogen Energy Storage System for Power-to-Gas and Gas-to-Power Systems. *J. Mod. Power Syst. Clean. Energy* **2023**, *11*, 885–895. https://doi.org/10.35833/MPCE.2021.000705.
15. Li, J.; Zhang, H.; Li, C.; et al. Modeling of Large-Scale Hydrogen Storage System Considering Capacity Attenuation and Analysis of Its Efficiency Characteristics. *Energy* **2024**, *121*, 291–313. https://doi.org/10.32604/ee.2023.027593.
16. Minuto, F.D.; Rozzi, E.; Borchiellini, R.; et al. Modeling Hydrogen Storage at Room Temperature: Adsorbent Materials for Boosting Pressure Reduction in Compressed H_2 Tanks. *J. Energy Storage* **2024**, *90*, 111758. https://doi.org/10.1016/j.est.2024.111758.
17. Rozzi, E.; Minuto, F.D.; Lanzini, A. Dynamic Modeling and Thermal Management of a Power-to-Power System with Hydrogen Storage in Microporous Adsorbent Materials. *J. Energy Storage* **2021**, *41*, 102953. https://doi.org/10.1016/j.est.2021.102953.
18. DeSantis, D.; Mason, J.A.; James, B.D.; et al. Techno-Economic Analysis of Metal–Organic Frameworks for Hydrogen and Natural Gas Storage. *Energy Fuels* **2017**, *31*, 2024–2032. https://doi.org/10.1021/acs.energyfuels.6b02510.
19. Peng, P.; Anastasopoulou, A.; Brooks, K.; et al. Cost and Potential of Metal–Organic Frameworks for Hydrogen Back-up Power Supply. *Nat. Energy* **2022**, *7*, 448–458. https://doi.org/10.1038/s41560-022-01013-w.
20. DOE Technical Targets for Onboard Hydrogen Storage for Light-Duty Vehicles. Available online: https://www.energy.gov/eere/fuelcells/doe-technical-targets-onboard-hydrogen-storage-light-duty-vehicles (accessed on 8 July 2025).
21. Huld, T.; Müller, R.; Gambardella, A. A New Solar Radiation Database for Estimating PV Performance in Europe and Africa. *Sol. Energy* **2012**, *86*, 1803–1815. https://doi.org/10.1016/j.solener.2012.03.006.
22. PUN Index GME. Available online: https://gme.mercatoelettrico.org/it-it/Home/Esiti/Elettricita/MGP/Esiti/PUN (accessed on 9 July 2025).
23. Electricity Price Statistics. Available online: https://ec.europa.eu/eurostat/statistics-explained/index.php?title=Electricity_price_statistics (accessed on 9 July 2025).
24. Ulleberg, O. *Stand-Alone Power Systems for the Future: Optimal Design, Operation and Control of Solar-Hydrogen Energy Systems*; Norges Teknisk-Naturvitenskapelige Universitet: Trondheim, Norway, 1998.
25. Harrison, K. *MW-Scale PEM-Based Electrolyzers for RES Applications: Cooperative Research and Development Final Report, CRADA Number CRD-18-00742*; National Renewable Energy Lab (NREL): Golden, CO, USA, 2021.
26. Rozzi, E.; Grimaldi, A.; Minuto, F.D.; et al. Model Complexity and Optimization Trade-Offs in the Design and Scheduling of Hybrid Hydrogen-Battery Systems. *Energy Convers. Manag.* **2025**, *344*, 120306. https://doi.org/10.1016/j.enconman.2025.120306.
27. Sdanghi, G.; Schaefer, S.; Maranzana, G.; et al. Application of the Modified Dubinin-Astakhov Equation for a Better Understanding of High-Pressure Hydrogen Adsorption on Activated Carbons. *Int. J. Hydrogen Energy* **2020**, *45*, 25912–25926. https://doi.org/10.1016/j.ijhydene.2019.09.240.
28. Li, B.; Wen, H.-M.; Zhou, W.; et al. Porous Metal-Organic Frameworks: Promising Materials for Methane Storage. *Chem.* **2016**, *1*, 557–580. https://doi.org/10.1016/j.chempr.2016.09.009.
29. Abdelkareem, M.A.; Abbas, Qaisar.; Mouselly, M.; et al. High-Performance Effective Metal–Organic Frameworks for Electrochemical Applications. *J. Sci. Adv. Mater. Devices* **2022**, *7*, 100465. https://doi.org/10.1016/j.jsamd.2022.100465.
30. da Silva, G.G.; Silva, C.S.; Ribeiro, R.T.; et al. Sonoelectrochemical Synthesis of Metal-Organic Frameworks. *Synth. Met.* **2016**, *220*, 369–373. https://doi.org/10.1016/j.synthmet.2016.07.003.

31. Wang, J.; Wang, Y.; Hu, H.; et al. From Metal–Organic Frameworks to Porous Carbon Materials: Recent Progress and Prospects from Energy and Environmental Perspectives. *Nanoscale* **2020**, *12*, 4238–4268. https://doi.org/10.1039/C9NR09697C.
32. Purewal, J.J.; Liu, D.; Yang, J.; et al. Increased Volumetric Hydrogen Uptake of MOF-5 by Powder Densification. *Int. J. Hydrogen Energy* **2012**, *37*, 2723–2727. https://doi.org/10.1016/j.ijhydene.2011.03.002.
33. Rozzi, E.; Minuto, F.D.; Lanzini, A. Techno-Economic Dataset for Hydrogen Storage-Based Microgrids. *Data Brief.* **2024**, *56*, 110795. https://doi.org/10.1016/j.dib.2024.110795.
34. Energia: MASE, Pubblicato Decreto CER. Available online: https://www.mase.gov.it/portale/-/energia-mase-pubblicato-decreto-cer (accessed on 11 July 2025).
35. Stolte, M.; Minuto, F.D.; Perol, A.; et al. Optimisation of Green Hydrogen Production for Hard-to-Abate Industries: An Italian Case Study Considering National Incentives. *Int. J. Hydrogen Energy* **2025**, *141*, 1294–1304. https://doi.org/10.1016/j.ijhydene.2025.03.008.
36. Stolte, M.; Minuto, F.D.; Lanzini, A. Optimizing Green Hydrogen Production from Wind and Solar for Hard-to-Abate Industrial Sectors across Multiple Sites in Europe. *Int. J. Hydrogen Energy* **2024**, *79*, 1201–1214. https://doi.org/10.1016/j.ijhydene.2024.07.106.
37. Pymoo—NSGA-III. Available online: https://pymoo.org/algorithms/moo/nsga3.html (accessed on 10 September 2025).
38. Giannuzzo, L.; Massano, M.; Schiera, D.S.; et al. Benchmarking Genetic Algorithms for Short-Term Battery Energy Storage Systems Optimization. In Proceedings of the 2025 IEEE 49th Annual Computers, Software, and Applications Conference (COMPSAC), Toronto, ON, Canada, 1 July 2025; pp. 2053–2059.
39. Alander, J.T. On Optimal Population Size of Genetic Algorithms. In Proceedings of the CompEuro 1992 Proceedings Computer Systems and Software Engineering, The Hague, The Netherlands, 4–8 May 1992; pp. 65–70.
40. EU 2023/1184. Available online: https://eur-lex.europa.eu/eli/reg_del/2023/1184/oj/eng (accessed on 23 July 2025).
41. EU 2023/1185. Available online: https://eur-lex.europa.eu/eli/reg_del/2023/1185/oj/eng (accessed on 23 July 2025).
42. Ramasamy, V.; Zuboy, J.; Woodhouse, M.; et al. *Solar Photovoltaic System and Energy Storage Cost Benchmarks, with Minimum Sustainable Price Analysis: Q1 2023*; National Renewable Energy Lab (NREL): Golden, CO, USA, 2023.
43. Farrell, J. *Questioning Solar Energy Economies of Scale*, 2015 ed.; Minneapolis, MN, USA: 2016.
44. Marocco, P.; Ferrero, D.; Lanzini, A.; et al. Optimal Design of Stand-Alone Solutions Based on RES + Hydrogen Storage Feeding off-Grid Communities. *Energy Convers. Manag.* **2021**, *238*, 114147. https://doi.org/10.1016/j.enconman.2021.114147.
45. Singla, M.K.; Gupta, J.; Beryozkina, S.; et al. The Colorful Economics of Hydrogen: Assessing the Costs and Viability of Different Hydrogen Production Methods—A Review. *Int. J. Hydrogen Energy* **2024**, *61*, 664–677. https://doi.org/10.1016/j.ijhydene.2024.02.255.